BIBLIOGRAPHIC INFORMATION SYSTEM

JOURNAL FULL TITLE: Journal of Biomedical Research & Environmental Sciences
ABBREVIATION (NLM): J Biomed Res Environ Sci **ISSN:** 2766-2276 **WEBSITE:** https://www.jelsciences.com

SCOPE & COVERAGE

- **Sections Covered:** 34 specialized sections spanning 143 topics across Medicine, Biology, Environmental Sciences, and General Science
- Ensures broad interdisciplinary visibility for high-impact research.

PUBLICATION FEATURES

- **Review Process:** Double-blind peer review ensuring transparency and quality
- **Time to Publication:** Rapid 21-day review-to-publication cycle
- **Frequency:** Published monthly
- **Plagiarism Screening:** All submissions checked with iThenticate

INDEXING & RECOGNITION

- **Indexed in:** Google Scholar, IndexCopernicus (**ICV 2022: 88.03**)
- **DOI:** Registered with CrossRef (**10.37871**) for long-term discoverability
- **Visibility:** Articles accessible worldwide across universities, research institutions, and libraries

OPEN ACCESS POLICY

- Fully Open Access journal under Creative Commons Attribution 4.0 License (CC BY 4.0)
- Free, unrestricted access to all articles globally

GLOBAL ENGAGEMENT

- **Research Reach:** Welcomes contributions worldwide
- **Managing Entity:** SciRes Literature LLC, USA
- **Language of Publication:** English

SUBMISSION DETAILS

- Manuscripts in Word (.doc/.docx) format accepted

SUBMISSION OPTIONS

- **Online:** https://www.jelsciences.com/submit-your-paper.php
- **Email:** support@jelsciences.com, support@jbresonline.com

HOME ABOUT ARCHIVE SUBMIT MANUSCRIPT APC

Vision: The Journal of Biomedical Research & Environmental Sciences (JBRES) is dedicated to advancing science and technology by providing a global platform for innovation, knowledge exchange, and collaboration. Our vision is to empower researchers and scientists worldwide, offering equal opportunities to share ideas, expand careers, and contribute to discoveries that shape a healthier, sustainable future for humanity.

JOURNAL OF BIOMEDICAL RESEARCH & ENVIRONMENTAL SCIENCES
ISSN: 2766-2276
SUBJECT AREA(S): PHYSICS | MATERIAL SCIENCE
DOI: 10.37871

REVIEW ARTICLE

Optical Properties of Excitons in CdSe Nanoplatelets

Czajkowski G*

Technical University of Bydgoszcz, Al. Prof. S. Kaliskiego 7, 85-789 Bydgoszcz, Poland

Abstract

We show how to calculate the linear and nonlinear optical functions of CdSe nanoplatelets, taking into account the effect of a dielectric confinement on excitonic states. We consider both stationary and non-stationary excitation regime. We obtain obtain analytical expressions for the absorption coefficient, the exciton resonance energy and binding energy of nanoplatelets. The impact of plate geometry (thickness, lateral dimension) on the spectrum is discussed. In the nonlinear case we analyze the impact of temperature. For the short-pulse excitation the time dependence of the spectra is considered. The results are compared with the available experimental data.

Introduction

The quantum size effects in semiconductor nanocrystals, first pointed out in 1981 [1] have unlocked plethora of research topics for semiconductor nanosystems [2]. The synthesise of nearly monodispersive semiconductor nanocrystallites, such as cadmium selenide (CdSe) [3,4] opened the way to producing nanosystems of various dimensions. Here we consider nanoplatelets (NPLs), which are cuboid shaped quantum dots where electrons and holes are confined in three dimensions, of a large lateral size but of only a few molecular layers of thickness. The carriers, electrons and holes, are strongly confined in the growth (z-) direction, and weakly confined in the plane. In the mostly considered CdSe NPL's the vertical confinement is of electrostatic origin and is caused by a large dielectric mismatch between the semiconductor (here CdSe) and its environment. The lateral confinement can be treated similar as in QWs, as a results of impenetrable barrier. Similar as in traditional QDots and QWs, electrons and holes interact by a screened Coulomb potential. The bound electron-hole pairs created by a propagating electromagnetic wave are

***Corresponding author(s)**

Czajkowski G, Technical University of Bydgoszcz, Al. Prof. S. Kaliskiego 7, 85-789 Bydgoszcz, Poland

Email: czajk@pbs.edu.pl

DOI: 10.37871/jbres2252

Submitted: 24 October 2025

Accepted: 13 November 2025

Published: 08 January 2026

Scan Me

How to cite this article: Czajkowski G. Optical Properties of Excitons in CdSe Nanoplatelets. J Biomed Res Environ Sci. 2026 Jan 08; 7(1): 19. Doi: 10.37871/jbres2252

named excitons and they determine the optical properties of the medium. Cadmium selenide NPLs, first fabricated in 2006 [5] have become important examples of a two-dimensional colloidal nanosystem, with large exciton binding energy, strong quantum confinement and huge oscillator strength, which allows for a high tunability of their optical properties [5]; they exhibit strong and narrow emission lines at both cryogenic and room temperatures. [6] The combined action of very small dimension in the z- direction (few monolayers), strong confinement potential, and Coulomb interaction leads to exciton binding energy reaching hundreds of meV (the bulk binding energy is only 15 meV); it is remarkable quality of CdSe NPLs, which strongly affects their optical properties. Recently several groups have measured the exciton binding energy of CdSe NPLs [6–8]. But the sole knowledge of excitonic binding energy is not sufficient to describe, interpret and explain the observed optical spectra. Beside of the huge binding energy, the are also another interesting effects. For example, Achtstein et al. [9] measured the population dynamics of excited state emission from p-states in CdSe NPLs. They also measured the temperature dependence of the emission dynamics. Similar phenomena have been recently analyzed in Cu_2O crystals for the even series of Rydberg excitons [10].

The recent growth o interest in such systems encourages us to present a method, which gives a simple analytical expression for optical functions, taking into account confinement and dielectric potentials and any excitonic states,

A majority of authors, describing theoretically the optical properties of excitons in NPLs, are using perturbation calculus, where unperturbed eigenfunctions, describing the carriers motion in the z-direction, are the (finite or infinite) 1-dimensional quantum well functions. The binding energy is then calculated with Coulomb e-h interaction potential considered as perturbation [11,12]. A numerical attempt to calculate electronic properties of CdSe NPLs spectra has also been taken by Benchamekh et al. [6] who applied an advanced tight-binding model. In the present work we propose a different confinement potential, resulting directly from the dielectric confinement. This potential allows for an analytical solution of the Schrödinger equation for electron and hole, describing their motion in the z-(confinement) direction. We obtain both eigenfunctions and eigenvalues. Adding the solution of the Schrödinger equation for in plane relative motion we can estimate the total binding energy. Moreover, we present the theoretical method which allows one to calculate optical properties (i.e., positions of resonances and absorption spectra) of NPLs depending on numbers of monolayers (i.e. thickness of NPLs) and the lateral extension. In calculations we have used the so-called real density matrix approach (RDMA), which allows one to obtain analytical expressions for the susceptibility. The method has been used extensively in bulk semiconductor materials, and has been also applied to various types of nanostructures, to compute linear and nonlinear optical properties (see, for example, Refs.[13–15]).

The first attempt to apply RDMA in the case of CdSe NPLs is given in Ref. [16]. We extend the approach from Ref.[16], adding results on the exciton states size dependence, and nonlinear effects, such as exciton population decay, and temperature dependence of the spectra.

The paper is organized as follows. In Sec. 2 we recall the basic equations of the used approach (RDMA). In Sec. 3 we present an approximation, which enables analytic calculations. The results obtained by the method are presented in Sections 4 and 5, containing excitonic resonance energies, binding energies, and absorption spectra for NPLs with different sizes, including the time- and temperature dependence of the absorption spectra. The last section presents

the concluding remarks. Appendix contains the details of analytical calculations.

Theory

We consider a CdSe nanoplatelet of cuboid shape, located at the z = 0 plane, and with the barriers located at $x = \pm L_x/2, y = \pm L_y/2, z = \pm L_z/2$. We consider the response of the NPL to a normally incident electromagnetic wave, linearly polarized in the x -direction

$$\boldsymbol{E}_i(z,t) = \boldsymbol{E}_{i0}(t)\exp(ik_0 z - i\omega t), \quad k_0 = \frac{\omega}{c}. \quad (1)$$

Since we will consider both stationary, and non-stationary excitation, the amplitude $E_{io}(t)$ is assumed in the form

$$\boldsymbol{E}(z,t) = \boldsymbol{E}_{i0}(t)F(t)\exp(ik_0 z - it) \quad (2)$$

where $F(t)$ describes the pulse shape in the case of non-stationary excitation. For a stationary excitation we put $F(t)$ = 1.

where $F(t)$ describes the pulse shape in the case of nonstationary excitation. For a stationary excitation F = 1. The calculations of the optical response in the framework of RDMA is based on the solution of the so-called constitutive equations for two-point correlation functions $Y(\mathbf{x}_e,\mathbf{x}_h)$, (inter-band transition amplitude, also called exciton amplitude), and $C(\mathbf{x}_e,\mathbf{x}_h)$, $D(\mathbf{x}_e,\mathbf{x}_h)$, (intra-band transitions), where $\mathbf{x}_e$;$\mathbf{x}_h$ are the electron and hole coordinates. The derivation and the explicite form of the constitutive equations can be found in Ref. [13]. The constitutive equations must be solved simultaneously with the Maxwell field equations

$$c^2\varepsilon_0\nabla\times\nabla\times E - \varepsilon_0\varepsilon_b\,\partial_t^2\boldsymbol{E} = \partial_t^2\boldsymbol{P}, \quad (3)$$

where $\boldsymbol{P}$ is the polarization, and ε_1 the NPL material dielectric constant. When the effects of confinement are considered, one makes use of the appropriate boundary conditions for $\boldsymbol{E}$,Y,C and D.

In the weak excitation field limit and for the linear case, where we put C = D = 0 on the right-hand side, we obtain equations for the intraband transition amplitudes $Y_{12}^{\alpha b}$ of the electron-hole pair of coordinates $\mathbf{x}_1 = \mathbf{x}_h$ and $\mathbf{x}_2 = \mathbf{x}_e$ between any pair of bands α and b have the form

$$-i(\partial_t + \Gamma_{\alpha b})Y_{12}^{\alpha b} + H_{eh\alpha b}Y_{12}^{\alpha b} = \boldsymbol{M}_{\alpha b}\boldsymbol{E} \quad (4)$$

where $\Gamma_{\alpha b} = \hbar/\tau^{\alpha b}, \tau^{\alpha b}$ is the exciton life time [10], and $\hbar = 0.6582\,meV\times ps$ the Planck constant.

The two-band Hamiltonian $H_{eh\alpha b}$ with energy gap $E_{g\alpha b}$ for any pair of bands reads

$$H_{eh\alpha b} = E_{g\alpha b} + (1/2m_\alpha)\,\boldsymbol{p}_{h\alpha}^2 + (1/2m_b)\,\boldsymbol{p}_{eb}^2 + V_{eh}(1,2) + V_h(1) + V_e(2), \quad (5)$$

with electron and hole kinetic energy operators, m_α and m_b being the band effective masses, V_{eh} describes the electron-hole attraction and V_e,V_h denote the confinement potentials of the electron and the hole, respectively. The total polarization of the medium is related to the excitonic amplitudes by

$$\boldsymbol{P}(\boldsymbol{X}) = 2\sum_{\alpha,\ldots,a,\ldots} Re\int d^3\times\boldsymbol{M}_{\alpha b}(\boldsymbol{x})Y_{12}^{\alpha b}(\boldsymbol{X},\boldsymbol{x}), \quad (6)$$

where $\mathbf{x}$ = $\mathbf{x}_e$ - $\mathbf{x}_h$ is the relative coordinate, and X the electron-hole pair center-of-mass coordinate, and the summation includes all allowed excitonic transitions between the valence and conduction bands.

For CdSe based NPLs we have to consider both heavy(H) and light(L) hole excitons. For the optical transitions between (α = H,L) valence bands and the conduction band (b = C) we get two constitutive equations for the excitonic amplitudes

$$Y_{12}^{\alpha C} = Y_\alpha(x_e,x_h)$$
$$-i\hbar\partial_t Y_\alpha - i\Gamma_\alpha Y_\alpha + H_{ehH}Y_\alpha = M_\alpha(x)E(X), \quad (7)$$

where $M_\alpha(x)$ are transition dipole densities. The operators $H_{eh\alpha}$ have the form

$$H_{ehH\alpha} = E_{g\alpha} + \frac{p_{hz}^2}{2m_{hz\alpha}} + V(1) + \frac{p_{ez}^2}{2m_{ez}} + V(2) \quad (8)$$

$$+ \frac{P_X^2}{2M_{\|\alpha}} + \frac{P_Y^2}{2M_{\|\alpha}} + \frac{p_{\rho_e}^2}{2\mu_{\|\alpha}} + \frac{p_{\rho_h}^2}{2\mu_{\|\alpha}} + V_{eh}(z_e - z_h, \rho),$$

where $V_{eh}(z_e - z_h,\rho)$ is the screened Coulomb interaction

$$V_{eh}(z_e - z_h, \rho) = \frac{-e^2}{4\pi\epsilon_0\epsilon_1\sqrt{\rho^2 + (z_e - z_h)^2}}, \quad (9)$$

f_{ESL}

are the reduced in plane effective masses for electron-hole pair, and $\rho_{e,h}$ are two-dimensional vectors in the x - y $x-y$ plane, $\rho_{e,h} = (x_{e,h}, y_{e,h})$,

$$\rho^2 = (\rho_e - \rho_h)^2 = (x_e - x_h)^2 + (y_e - y_h)^2. \quad (10)$$

We have separated the center-of-mass coordinate $X_{||}$ and the related momenta P_x, P_y from the relative coordinates $\rho_{e,h}$ on the plane (x,y) and the related momenta p_{ρ_e}, p_{ρ_h}.

$$M_{\|\alpha} = m_{h\|\alpha} + m_{e\|}$$

is the total in-plane exciton mass, $\rho_e - \rho_h$ is the relative electron-hole coordinate in the x - y plane. Using Hamiltonian (8), with the harmonic time dependence $\propto \exp(-i\omega t)$ we obtain the constitutive equations in the form

$$(H_{eh\alpha} - \hbar\omega - i\Gamma_\alpha) Y_\alpha(\rho_e, \rho_h, z_e, z_h) \quad (11)$$

$$= M_\alpha(\rho, z_e, z_h) E(X_\|, Z).$$

Note that the above equation refers to a 6-dimensional space. In spite of the symmetry differences between the confinement potentials and the Coulomb potential, an analytic solution of Eq. (11) not exists. Therefore several approximations have been used. One of them is to seek the solution as a product of eigenfunctions of one-dimensional infinite-deep confinement potential,

$$\psi\left(x_i^{c,v}\right) = \sqrt{\frac{2}{L_i}} \sin\left(\frac{\pi n_i^{c,v}}{L_i}\right), \quad (12)$$

where $x_i^{c,v} = x_e, y_e, \ldots z_e, z_h$.

The functions (12) are then used within the framework of perturbation theory [11,12]. In the next section we show how, with certain simplifying assumptions, the dimensionality of the problem can be reduced from 6 to 3, enabling to obtain analytical solution of the linear inter-band equation (11) with respective exciton resonance energies.

Approximate solution of the linear constitutive equation

To reduce the dimensionality of our problem, following simplifications are assumed.

1. Since, in the case of CdSe, the effective mass of the hole is much larger than that of the electron, we neglect the effects of the lateral motion of the hole, considered it as located in the center of the NPL. Similar assumptions were made in the past in the case of Quantum Dots [17], and Quantum Disks [16,18].

2. We assume, that the optical properties of a rectangular NPL can be described by a motion of the electron in a cylindrical disk with the radius

$$r_{eff} = \sqrt{\frac{L_x \cdot L_y}{\pi}}. \quad (13)$$

3. The confinement potential for the motion of the electron in x - y plane is given by expression

$$V_e(\rho_e) = \begin{cases} 0 & for \quad \rho_e \le R, \\ \infty & for \quad \rho_e > R. \end{cases} \quad (14)$$

where we put $R = r_{eff}$. For the further calculations we will need the eigenfunctions and eigenvalues

of a two-dimensional Schrödinger equation

$$\left[\frac{p_{\|}^2}{2m_{e_{\|}}} - \frac{e^2}{4\pi\epsilon_0\epsilon_1\rho_e} + V_e(\rho)\right]\psi(\rho_e) = E\psi(\rho_e), \quad (15)$$

satisfying the boundary condition $\psi(r_{eff}) = 0$. The electron inside the disk is subject to two competing forces: the repulsive (confinement) force, connected with a positive energy, and the attractive Coulomb force (attraction by the hole), related to a negative energy. Therefore the eigen-energy E_{jm}, being the sum of the mentioned contributions, can be positive, negative, or zero. For the negative energies, we have [18]

$$\psi_{jm}(\xi,\phi) = C\xi^{|m|}e^{-\xi/2} \quad (16)$$

$$\times M\left(m + \frac{1}{2} - \eta, 2|m|+1; \xi\right)\frac{e^{im\phi}}{\sqrt{2\pi}},$$

where j and m are the principal and magnetic quantum numbers of the excitonic state, $M(a,b,z)$ is the confluent hypergeometric function (notation by Ref. [19]), $= \rho_e$,

$$\eta = \frac{2}{k}, \quad \xi = k\rho, a_{e\|}^* = \frac{m_0}{\epsilon_1}a_B^*,$$

$$k^2 = -4\frac{2m_{e\|}}{\hbar^2}a_{e\|}^{*2}E = -4/\epsilon,$$

Where m_0 is the free electron mass, and

$$a_B^* = 0.0529\,nm$$

the hydrogen Rydberg radius. The quantities k, ρ, and ξ are dimensionless (defined in the parameters related to the electron). The eigenfunction, due to the no escape boundary condition (14), satisfies the equation

$$\psi_{jm}(k\rho_{eff},\phi) = 0, \quad \rho_{eff} = \frac{r_{eff}}{a_{e\|}^*}, \quad (17)$$

giving the eigenenergies E_{jm}, m = 0,1,..., j = 0,1,... (75). In the case of positive energy, the electron eigenfunction has the form

$$\psi_{jm}(\xi,\phi)) = Ce^{-i\xi/2}\xi^{|m|}$$

$$\times M\left(|m|+\frac{1}{2} - i\eta, 2|m|+1; i\xi\right), \quad (18)$$

with a normalization constant C. The eigenenergy can be calculated from the condition

$$Re\psi_{jm}(\mathcal{R}) = 0. \quad (19)$$

The positive eigenenergies are then given by

$$\varepsilon = \frac{1}{\eta^2}R_{e\|}^*. \quad (20)$$

4. The movement of electrons and the holes in the z direction is affected by the dielectric confinement potential, which we take in the form

$$V_{e,h}(z) = \frac{\gamma_{e,h}}{(L/2) - z}. \quad (21)$$

The coefficient γ is proportional to dielectric coefficients [20,21]

$$\gamma \propto \frac{\epsilon_1 - \epsilon_2}{\epsilon_1(\epsilon_1 + \epsilon_2)},$$

where ε_2 and ε_1 are the dielectric constants of external and internal media, respectively, and $\epsilon_2 << \epsilon_1$. Using the potential (21), we solve the Schrödinger equation

$$-\frac{\hbar^2}{2m_z}\frac{d^2}{dz^2}\psi_{e,h}(z) + \frac{\gamma R_z^* a_z^*}{(L/2) - z}\psi_{e,hN}(z)$$

$$= E_z\psi_{e,h}(z), \quad (22)$$

where m_z denotes the effective mass of the considered quasi particle (electron or hole) in the z-direction, R_z^*, a_z^* are the corresponding effective Rydberg energies, and Bohr radii defined as

$$R^*_{e,hz} = \frac{m_{e,hz} e^4}{2(4\pi\epsilon_0\epsilon_1)^2\hbar^2} \tag{23}$$

$$= \left(\frac{m_{e,hz}}{m_0}\right)\frac{1}{\epsilon_1^2} R^*_B,$$

$$a^*_{e,hz} = \frac{\hbar^2(4\pi\epsilon_0\epsilon_1)}{m_{e,hz} e^2} = \left(\frac{m_0}{m_{e,hz}}\right)\epsilon_b a^*_B, \tag{24}$$

where $R^*_B = 13600$ meV is the hydrogen Rydberg energy. The eigenfunctions and eigenvalues have the form [16]

$$\psi(u) = Cu e^{-u/2} M\left(1-\lambda, 2; u\right), \tag{25}$$

with the normalization constant C. The following notation is used

$$d = \frac{L}{2a^*_z}, \quad \zeta = \frac{d-z}{a^*_z},$$

$$\varepsilon = \frac{E}{R^*}, \quad k = \frac{2}{\sqrt{\epsilon}}, \quad u = -ik\zeta. \tag{26}$$

The eigenvalues follow from the condition

$\psi(-ikd) = 0$ and, in the lowest approximation, have the form

$$E_{e,hz} = \frac{6\beta[1+(\gamma_{e,h} d_{e,h}/2)]}{m_{e,hz} L^2}, \tag{27}$$

with β $\beta = a^{*2}_B \times R^*_B = 38 nm^2 \cdot meV,$ (28)

where $[L] = nm$.

Using the above defined eigenfunctions, we define $Y(\rho_e, z_e, z_h)$ as a series

$$Y = \sum_{jm} Y_{0jm} \psi_{jm}(\rho_e)\psi_e(z_e)\psi_h(z_h), \tag{29}$$

with certain coefficients Y_{0jm}. We restricted the consideration to the lowest confinement functions in the z direction. We substitute the expansion into Eq. (11), which is transformed to the form

$$\mathcal{H} Y = ME - \Delta V Y, \tag{30}$$

where

$$\mathcal{H} = E_g + E_g + \frac{p^2_{ez}}{2m_{ez}} + V_e(z_e) + \frac{p^2_{hz}}{2m_{hz\alpha}} \tag{31}$$

$$+V_h(z_h) + \frac{p^2_{e\|}}{2m_{e\|}} + V_e(\rho_e) - \frac{e^2}{4\pi\epsilon_1\rho_e} - i\Gamma_\alpha,$$

and

$$\Delta V = \frac{e^2}{4\pi\epsilon_1\rho_e} - \frac{e^2}{4\pi\epsilon_1\sqrt{\rho_e^2 + (z_e - z_h)^2}}. \tag{32}$$

Eq. (30) can be solved by means of a Green's function appropriate to the l.h.s. operator in (30), satisfying the equation

$$\{E_g - \hbar\omega - i\Gamma + \frac{p^2_{ez}}{2m_{ez}} + \frac{p^2_{hz}}{2m_{hz}} + V_e(z_e) + V_h(z_h)$$

$$+ \frac{p^2_{\|}}{2m_e} - \frac{e^2}{4\pi\epsilon_0\epsilon_1\rho}\} G(\rho, \sigma, \varphi, \phi, z_e, w_e, z_h, w_h)$$

$$= -\frac{\delta(\rho-\sigma}{2\pi\rho}\delta(z_e - w_e)\delta(z_h - w_h)\delta(\varphi - \phi). \tag{33}$$

Making use of scaled variables (m_e scaled in m_0)

$$\rho = \frac{\rho_e}{a^*_{e\|}}, \quad a^*_{e\|} = \left(\frac{m_0}{m_{e\|}}\right)\epsilon_b a^*_B,$$

we obtain the Green function in the form

$$G = \frac{1}{2\pi}\psi_e(z_e)\psi_e(w_e)\psi_h(w_h)\psi_h(z_h)$$

$$\times \sum_{j,m} \frac{1}{k^2_{jm}} \psi_{jm}(\rho)\psi^*_{jm}(\sigma), \tag{34}$$

where

$$k^2_{jm} = \frac{2m_{e\|}}{\hbar^2}\left(E_g - \hbar\omega - i\Gamma_\alpha + E_{conf} + E_{jm}\right). \tag{35}$$

The quantities E_{conf} result from Eq. (27)

$$E_{conf} = E_{ez} + E_{hz}. \tag{36}$$

The solution of Eq. (30) reads

$$Y = GME - G(\Delta V)Y, \tag{37}$$

which is called the Lippmann-Schwinger equation. Inserting (29) into Eq. (37), with regard to (34), we obtain for a chosen state *jm*

$$Y_{0\,jm} = \frac{\langle \psi_{jm}(\rho)\psi_e(z_e)\psi_h(z_h) \mid ME\rangle}{Q_{jm}}. \tag{38}$$

The resonant denominator has the form

$$Q_{jm} = E_g + E_{conf,L_z} + E_{jm} + < \frac{2}{\rho} > \tag{39}$$

$$- < \frac{2}{\sqrt{\rho^2 + (z_e - z_h)^2}} > -\hbar\omega - i\Gamma,$$

with

$$< \frac{2}{\rho} >= 2R^*_{\|\alpha} \int_0^R \psi^2_{jm}(\rho)\rho d\rho \tag{40}$$

$$\times \int_0^1 dz_e \int_0^1 dz_h \psi^2_e(z_e)\psi^2_h(z_h),$$

$$E_{b,jm\alpha} = - < \frac{2}{\sqrt{\rho^2 + \mathcal{L}^2(z_e - z_h)^2}} >$$

$$= -2R^*_{\|\alpha} \int_0^R \rho d\rho\, \psi^2_{jm}(\rho) \tag{41}$$

$$\times \int_0^1 \int_0^1 \frac{dz_e dz_h \psi^2_e(z_e)\psi^2_h(z_h)}{\sqrt{\rho^2 + \mathcal{L}^2(z_e - z_h)^2}} =,$$

where $E_{b,jm\alpha}$ is called the exciton binding energy at the state *j*,*m*. The eigenvalues E_{jm} are defined in **Equations** (75) and (76), $\mathcal{L} = L / a^*_{e\|}$. Introducing a total confinement energy

$$E_{conf,tot,jm,\alpha} = E_g + E_{conf,L_z,\alpha} + < \frac{2}{\rho} > + E_{jm}, \tag{42}$$

we rewrite Eq. (39) to the form

$$Q_{jm\alpha} = E_{res,jm\alpha} - \hbar\omega - i\Gamma_\alpha, \tag{43}$$

where

$$E_{res,jm\alpha} = E_{conf,tot,jm,\alpha} + E_{b,jm,\alpha} \tag{44}$$

is the exciton resonance energy at the state *jmα*.

With the use of the above quantities we obtain the amplitudes Y_α, determining the NPL polarization by Eq. (6), which has the form

$$\chi = \frac{2}{\epsilon_0} \tag{45}$$

$$\times \sum_{jm,\alpha} \frac{|\langle M(\rho, z_e, z_h) \mid \psi_{jm}(\rho)\psi_e(z_e)\psi_h(z_h)\rangle|^2}{E_{res,jm,\alpha} - \hbar\omega - i\Gamma_{jm,\alpha}}.$$

The susceptibility (45) enables one to obtain the NPL's optical functions (absorption, reflection, and transmission coefficients).

Results of the Specific Calculations

Experiments Ref. [9]

We have performed calculations for CdSe NPLs having in mind the experimental results by Brumberg *et al.*[12], and Achtstein *et al.* [9] and. In this works two types of measurements are performed. In Ref. [9] PL emission of CdSe NPLs with fixed thickness (L_z) and various lateral dimensions has been measured. In Ref. [12] absorption spectroscopy in pulsed magnetic fields for three different CdSe NPL thicknesses and lateral areas is implemented. We analyze the both cases, calculating the size dependent exciton states energies, and displaying the related emission/absorption line shapes.

The basic ingredients used in the calculations are the band-gap data (band-gap energy, electron and hole effective masses, longitudinal-transverse energy), supplemented with the 'in' and 'out' dielectric constants ε_1 and ε_2. We follow the estimation of electron and hole effective masses, given in Ref. [16]. Other

Table 1: Masses, reduced masses, Rydberg energies, Luttinger parameters, and coherence radii, from Ref. [16].

Parameter	3ML	4ML	5ML
L	1	1.33	1.67
$a^*_{e\|\|}$	0.2567	0.2015	0.1635
r_{eff}	0.3208	0.2519	0.2044
m_{hzH}	1.1925	0.9754	0.8153
$1SH$	0.4957	0.4337	0.3879
m_{hzL}	0.4149	0.3659	0.3302
$m_{h\|\|L}$	0.8121	0.6887	0.5963
μ_{zH}	0.2112	0.1670	0.1362
$\mu_{\|\|H}$	0.1948	0.1593	0.1338
μ_{zL}	0.1586	0.1300	0.1094
$\mu_{\|\|L}$	0.2300	0.1844	0.1522
$R^*_{\|\|H}$	73.58	60.20	51.28
$R^*_{\|\|L}$	86.88	69.67	57.49
γ_1	1.6243	1.8789	2.1062
γ_2	0.3929	0.4269	0.4488
$a^*_{e\|\|}$	0.989	1.26	1.55
ρ_{0H}	0.20	0.18	0.17
ρ_{0L}	0.22	0.19	0.18

Table 2: Binding energies and exciton resonance energies calculated for lateral 5ML disk, thickness $L_z = 1.67nm$, analyzed by Achtstein. *et al*. [9], lengths in nm, masses in free electron mass, energies in meV, the energy gap at 4 K temperature 1840 meV, notation: 1: 8.1×3.6, 2: 17×6, 3: 21×7, 4: 29×8, 5: 41×13, 6: 30×15.

lat. extension	1	2	3	4	5	6
$m_{e\|\|}$	0.2044	0.2044	0.2044	0.2044	0.2044	0.2044
$R^*_{e\|\|}$	77.2					
$a^*_{e\|\|}$	1.553					
r_{eff}	3.05	5.7	6.84	8.59	13.13	11.96
λ	1.96	3.67	4.4	5.53	8.38	7.7
$E_{conf,tot}(1SH)$	1097.68	1013	1001	993	986.5	979.62
$E_{conf,tot}(2SH)$	1210.18	793.77	764.27	741.32	723.04	720.11

$E_{conf,tot}(1PH)$	839.88	760.84	744.4	729.7	716.55	714.4
$E_{conf,tot}(2PH)$	831.2	769.94	768.47	768.57	727.29	722.46
$E_{conf,tot}(1SL)$	1249.68	1165	1153	1145	1138.5	1131.62
$E_{conf,tot}(2SL)$	1362.18	945.77	916.27	893.32	875	872.11
$E_{conf,tot}(1PL)$	991.8	912.84	896.4	881.7	868.55	866.4
$E_{conf,tot}(2PL)$	1346.2	921.94	920.47	920.57	879.29	874.46
$\lvert E_b(1SH)\rvert$	391.16	362	359.3	358	357.3	354.88
$\lvert E_b(2SH)\rvert$	299.4	104	87.3	75.4	67.7	66
$\lvert E_b(1PH)\rvert$	153.9	100.8	91.5	83	75.14	74
$\lvert E_b(2PH)\rvert$	100	104.7	102.9	101.14	69.5	59.91
$E_{res}(1SH)$	2555.11	2491	2481.7	2475	2469.2	2464.7
$E_{res}(2SH)$	2750.8	2529.7	2517	2506	2495.3	2494.1
$E_{res}(1PH)$	2493	2500	2493	2486.7	2480.4	2481.6
$E_{res}(2PH)$	2571.2[a]	2503.0	2507	2507	2498	2502
$E_{res}(1SL)$	2707.11	2643	2633.7	2627	2621.2	2616.7
$E_{res}(2SL)$	2902.8	2681.7	2669	2658	2647.3	2646.2
$E_{res}(1PL)$	2645	2652	2645	2638.7	2633.5	2632.3
$E_{res}(2PL)$	2723.2	2659.4	2659.25	2659.4	2656.6	2655.55

Table 3: Exciton resonance energies at room temperature, calculated for lateral 5ML disk with the energy gap at room temperature (1750 meV [22]), notation: 1: $L_z = 1.67nm$, 2: 17×6, 3: 21×7, 4: 29×8, 5: 41×13 , 6: 30×5.

lat. extension	1	2	3	4	5	6
$E_{res}(1SH)$	2484.6	2401	2391.7	2385	2379.2	2374.7
$E_{res}(2SH)$	2660.8	2439.7	2427	2416	2405.3	2404.1
$E_{res}(1PH)$	2435.9	2410	2403	2396.7	2390.4	2391.6
$E_{res}(2PH)$	2416	2413	2417	2417	2408	2412
$E_{res}(1SL)$	2636.6	2553	2543.7	2537	2531.2	2526.7
$E_{res}(2SL)$	2812.8	2591.7	2579	2568	2557.3	2556.2
$E_{res}(1PL)$	2587.9	2562	2555	2548.7	2543.5	2542.3
$E_{res}(2PL)$	2568	2569.4	2569.25	2569.4	2566.6	2565.55

parameters are collected in Tables 1-4.

We start with the results from Ref. [9], where the NPLs of thickness 4.5 ML (we take 5 ML in calculations) and lateral dimensions ranging from 8×3.6 to 3015, are considered, (dimensions in nm). Using **Equations** (??) and (44), we have computed the exciton resonance energies and binding energies of heavy-hole exciton states 1SH (j = 0, m = 0), 2S (j = 1, m = 0), and 2PH (j = 0, m = 1). For the hole masses we used the data appropriate to the heavy- and light hole excitons (α = H, L). The results are presented in Table 1. Comparing the theoretical and experimental results from Ref. [9] (Table 5) we observe a very good agreement

In the next step we calculate the NPLs absorption spectrum. In the considered NPLs widths the typical wavelength of the input electromagnetic wave is much larger than the NPLs width, so we can use the long wave approximation. For further calculations we need to define the dipole density function **M**. The transition dipole density $M(\rho)$ should have the same symmetry properties as the solution of the corresponding Schrödinger equation. Since we focuss our attention on S and P states, we assume, the dipole density in the form

$$M_{GS}(r) = M_{0,GS\alpha} N_{GS} \exp(-\rho/\rho_{0\alpha})\delta(z_e - z_h), \quad (46)$$

for S states (ground state), and

$$\boldsymbol{M}_{ES}(\mathbf{r}) = \boldsymbol{M}_{0,ES,\alpha}\rho\delta(z_e - z_h)e^{-\rho/\rho_{0\alpha}} e^{i}/\sqrt{2\pi}, \quad (47)$$

for P (excited states) states, where $\rho_{0\alpha}$ are the so-called coherence radii

$$\rho_{0H} = \sqrt{\frac{R^*_{\|H}}{E_g}}, \quad \rho_{0L} = \sqrt{\frac{R^*_{\|L}}{E_g}}, \quad (48)$$

and N_{GS}, N_{ES} are normalization constants such that, for example,

$$N_{GS}\int_0^{\mathcal{R}} \rho\exp(-\rho/\rho_{0\alpha})d\rho = 1. \quad (49)$$

The dipole matrix elements $M_{0,GS\alpha}$, $M_{0,ES\alpha}$ are known in the case of bulk semiconductors, and their values are related to the so-called Longitudinal-Transversal splitting energy. The latter can be measured using the polariton dispersion relation. In the 2-dimensional systems with lateral confinement, and for normal incidence, we have no polaritons, and the dipole matrix elements are unknown. To estimate them, we use an expression based on the definition of the matrix elements between the hole and electron states j,j', adapted for the 2-dimensional case

$$M_{jmj'm'} = -e\iint d^2\rho_e \psi_j(\rho_e) \quad (50)$$
$$\times d^2\rho_h \psi_{j'}\rho_h(\rho_e - \rho_h)$$

with two-dimensional vectors $\rho_{e,h}$. With regard to the assumption of the hole located at the NPL center we arrive at

$$M_{jmj'm'} = -e\int d^2\rho_e \psi_j(\rho_e)\rho_e. \quad (51)$$

The results for various lateral extensions are displayed in Table 4. The radial damping parameters $\Gamma(GS, ES, r)$ in Table 4 result from the fitting to results of [9], where one reads

$$\Gamma_{ES} = 10.32 \quad for \quad S = 29\times 8,$$
$$= 32.24 \quad for \quad S = 41\times 13. \quad (52)$$

The ground state damping parameters are 2.43 meV and 4.2 meV for analogous lateral areas. The above values can be fitted by expressions

$$\Gamma_{ES} = A_{ES}\exp\left(-0.0008r_{eff}^2 + 0.2692r_{eff}\right),$$
$$\Gamma_{GS} = A_{GS}\exp(0.0084r_{eff}^2 - 0.0628r_{eff}), \quad (53)$$
$$A_{ES} = 1.102,\ A_{GS} = 2.2567.$$

With the above definitions we have all elements to calculate the mean NPL susceptibility, which can be written in the form

Table 4: Oscillator strengths and damping parameters for 1S, 2S, and 1P excitons for NPLs with dimensions as in Table 1: 1: $L_z = 1.67nm$, 2: 17×6, 3: 21×7, 4: 29×8, 5: 41×13, 6: 30×15, K_s by (56), $s = 1,\ldots,6$, dipole matrix elements M in $e \cdot nm$.

lat. extension	1	2	3	4	5	6
$M_{0,GS}$	0.5	0.434	0.389	0.322	0.2246	0.241
f_{GSH}	5.735	5.136	5.078	5.044	4.94	5.015
$M_{0,ES}$	1.63	2.34	2.625	2.88	3.09	3.1
f_{ESH}	0.104	0.16	0.124	0.0967	0.0738	0.0766
f_{GSL}	5.37	4.84	4.78	4.74	4.68	4.73
f_{ESL}		0.17	0.134	0.1	0.074	0.082
$\Gamma(GS,r)(4K)$	2.01	2.07	2.018	2.44	4.21	3.54
$\Gamma(GS,r)(273K)$	4.74	4.8	4.748	5.17	6.94	6.27
$\Gamma(ES,r)(4K)$	2.49	4.98	6.69	10.49	32.91	cc24.63
$\Gamma(ES,r)(273K)$	5.25	7.76	9.42	13.3	35.73	27.47
$\Gamma(GS,nr)(4K)$	0.016	0.0165	0.0161	0.02	0.04	0.028
$\Gamma(ES,nr)(4K)$	0.02	0.04	0.053	0.1	0.184	0.14
K_{sH}	0.19	0.9	1.11	1.53	2.82	2.41
K_{sL}	0.19	0.96	1.2	1.59	2.95	2.7
$K_{sH}\Gamma_{GS}\Gamma_{ES}(4K)$	4.56	9.37	14.98	39.46	391	211
$K_{sH}\Gamma_{GS}\Gamma_{ES}(273K)$	22.4	33.52	49.51	105.2	700	415
$K_{sL}\Gamma_{GS}\Gamma_{ES}(4K)$		9.89	16.2	40.7	409	235
$K_{sL}\Gamma_{GS}\Gamma_{ES}(273K)$		35.76	54	109.3	731.5	465

Table 5: Sizes and exciton states energies of CdSe NPLs from Ref. [9].

lat. extension/ energies	1SH	2SH	1PH	2PH	1SL
8.1×3.6	2574.6	2750	2512		
17×6	2491	2530	2500	2505	2643
21×7	2482	2517	2493	2505	2634
29×8	2475	2506	2487	2507	2627
30×15	2469	2495	2481	2498	2621
41×13	2464.7	2494	2480	2502	2616.7

$$\overline{\chi} = \frac{1}{L_z}\frac{2}{\epsilon_0}\int_{NPL} d^3r\, Y(r)M(r). \qquad (54)$$

The results, for L_z = 1.67 *nm*, and the lateral extensions for NPLs from Ref.[9], are displayed in Table 4.

Making use of the **Equantions** (6), (29),(38), (46), (47), and taking into account the relevant resonances $E_{res,j}$, we obtain the susceptibility of the considered CdSe NPL by **Equation** (45). The experiments in Ref. [9] were performed for excitation energy in the region of the 1SH (Ground State GS) and 1PH (Excited State ES) excitonic resonances. Therefore, using **Equation** (45), and with regard to normalization, we calculated the absorption(emission) coefficient by the formulas

$$\alpha_s = \frac{\Gamma_{GS}^2}{[E_{res,GS} - E_i]^2 + \Gamma_{GS}^2}$$

$$+K_s \frac{\Gamma_{GS}\Gamma_{ES}}{[E_{res,ES} - E_i]^2 + \Gamma_{ES}^2}, \qquad (55)$$

where s counts the NPLs (s = 1,...6 for the case of Ref. [9]), and

$$K_s = \frac{f_{ES}M_{0,ES}^2}{f_{GS}M_{0,GS}^2}. \qquad (56)$$

The results are displayed in **Figures** 1-6. In **Figure 1** we observe an inversion of states: the excited state is red shifted compared to the ground state. This is an effect which can be attributed to the competition of the confinement and the Coulomb attraction. For the smallest NPL the radius r_{eff} is smaller than the critical radius for the P excitons, it means that the confinement energy prevails over the Coulomb energy, which in effect gives the shift of resonance towards lower energies. For larger NPL extensions the situation is 'normal', it means the P exciton (ES) resonance has a larger energy than the GS resonance. We observe a fairly good agreement with experimental results by Achtstein *et al.* [9]. We also observe a decreasing of ES-GS intensity ratios with increasing NPL area, as was observed in experiments.

When the excitation energy interval increases, higher excited states should be taken into account. In particular, we observe the appearance light-hole 1SL and 1PL excitonic resonances, which have comparable oscillator strengths with the 1SH and 1PH excitons. It is illustrated in **Figures** 7-11.

Experiments Ref. [12]

In Ref. [12] absorption spectra at room temperature were measured for two 2 sets of CdSe NPLs, assorted according either to their thickness ('Thickness'), or lateral area ('Lateral Area').

The calculated spectra are shown in **Figures** 11 and 12. We obtained a fairly good agreement with experimental spectra. The dominating resonances are due to 1SH and 1SL excitons, and are slightly blue-shifted compared with the observed resonance energies. The differences can be explained in the following way. The above given dimensions were described as 'representative'. It means that in experiments different dimensions could be used, which can explain the differences between the theoretical and experimentally measured exciton resonance energies. Moreover, the effective electron and hole masses used through this section were calculated for NPL thicknesses 1, 1.33, and 1.67 nm, whereas in Ref. [12] the thicknesses 0.9, 1.2 and 1.5 nm were used. This also can be reason for the mentioned differences.

Time dependence

Here we refer to the experiments by Achtstein *et al.*, where the transient PL decay and evolution of the ES and GS emission with time were examined. The NPLs were irradiated by a short-pulse signal, with the pulse duration of 2 ps. We assume, that the pulse has a Gaussian

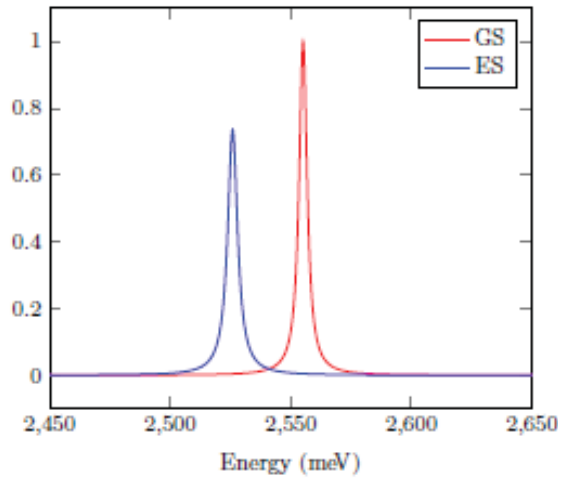

Figure 1 Normalized PL emission for lateral extension 8.1 × 3.6 at 4 K.

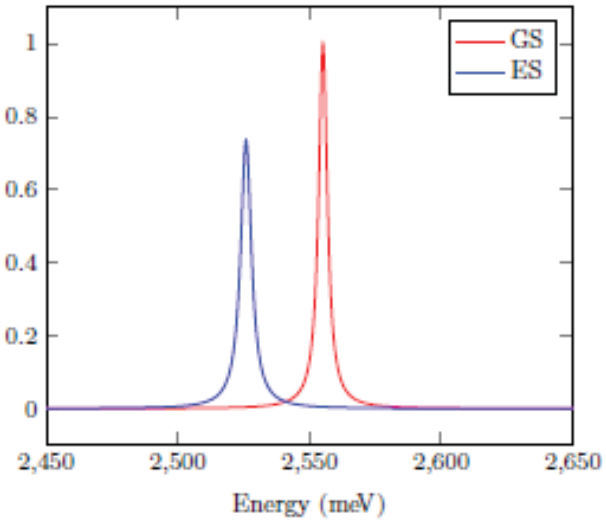

Figure 2 The same as Figure 1, for lateral extension 17×6.

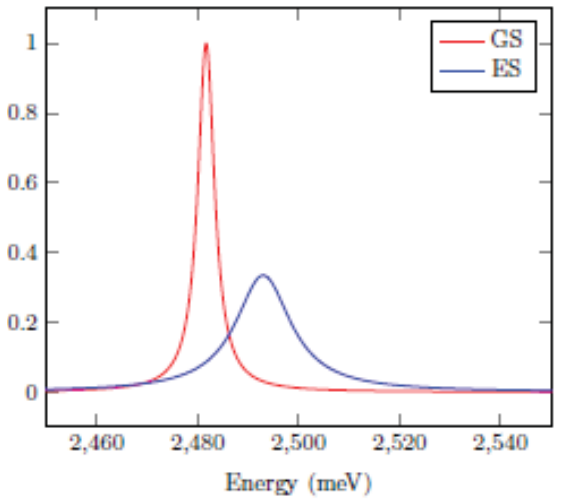

Figure 3 The same as Figure 1, for lateral extension 21 × 7.

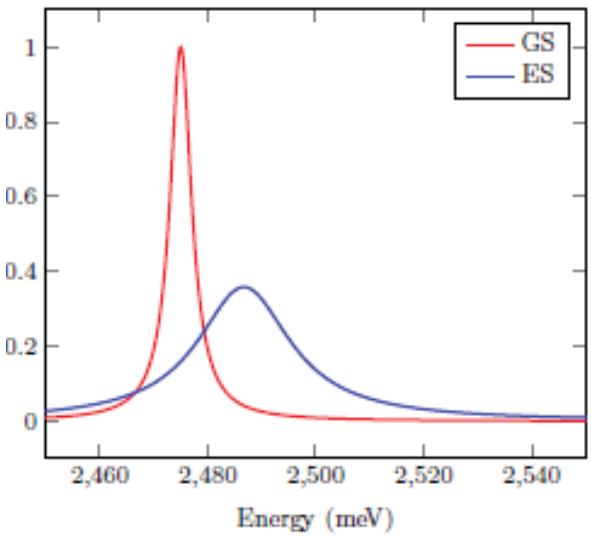

Figure 4 Lateral extension 29 × 8.

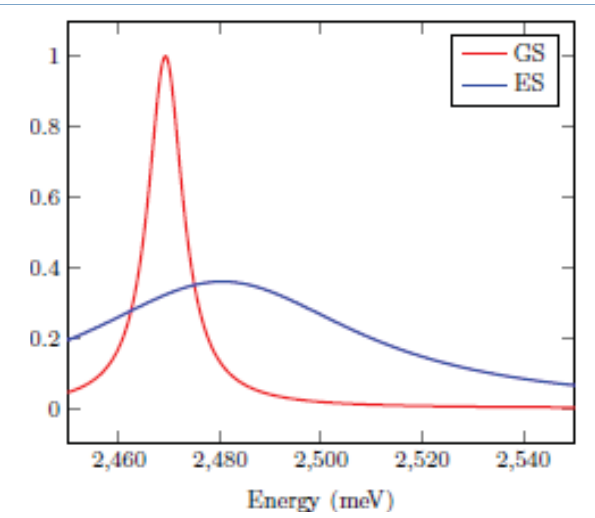

Figure 5 The same as Figure 1, for lateral extension 41 × 13.

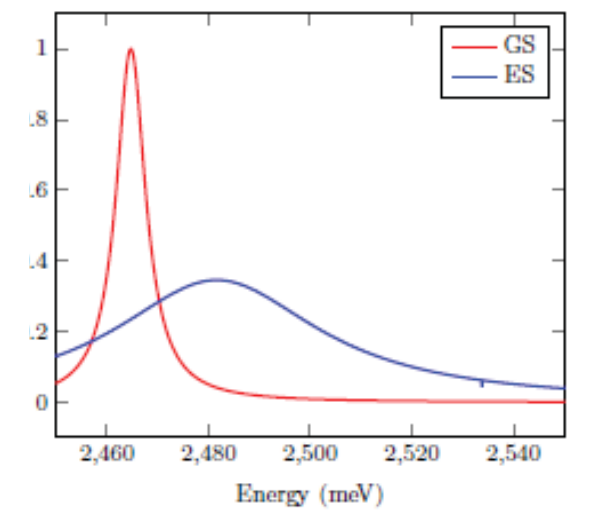

Figure 6 The same as Figure 1, for lateral extension 30×15.

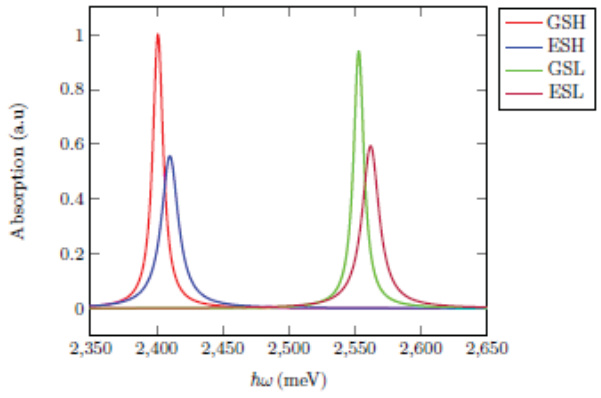

Figure 7 Normalized absorption, lateral extension 17×6 at 273 K.

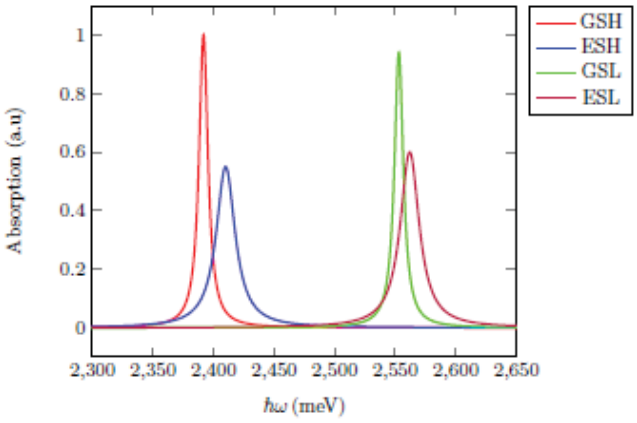

Figure 8 Normalized absorption for lateral extension 21×7at 273 K.

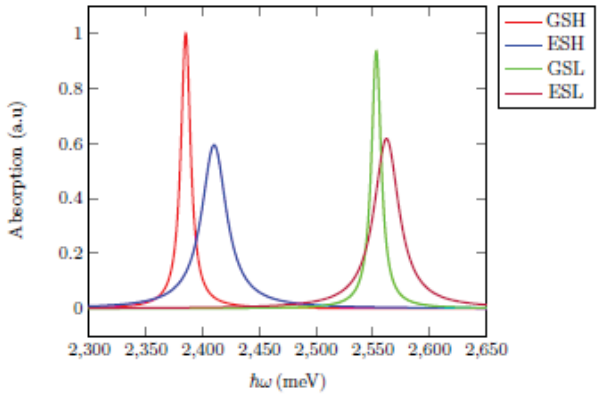

Figure 9 Normalized absorption for lateral extension 29×8 at 273 K.

shape

$$F(t) = F_{max} \frac{1}{\tau_p \sqrt{2\pi}} \exp\left(-\frac{t^2}{2\tau_p^2}\right), \qquad (57)$$

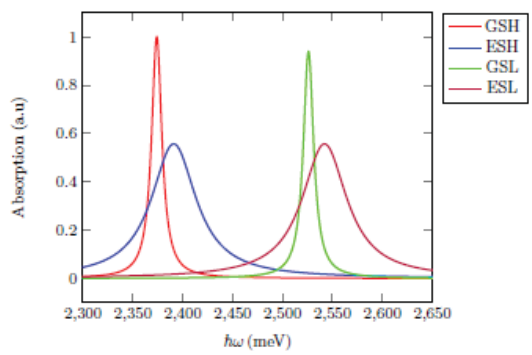

Figure 10 Normalized absorption for lateral extension 30 × 15 at 273 K.

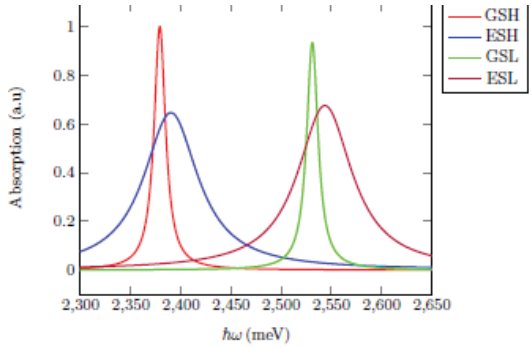

Figure 11 Normalized absorption for lateral extension 41×13 at 273 K.

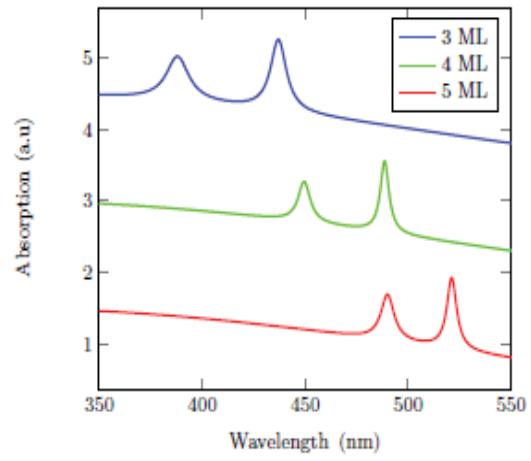

Figure 12 Normalized absorption for the case 'Thickness' at 273 K.

Where τ_p is the pulse temporal duration. Inserting the above pulse shape into Equation (1), we separate the excitonic amplitudes Y_α into two parts, slow and rapid. The processes of the excitonic creation are rapid processes, on the femtosecond scale. The decline process is

proportional to the exciton life time, which is of the order of a few ps, i.e. is a slow process. Moreover, one has two exciton life times, related to radiative (r), and non-radiative (nr) declines. For the slow counterpart of the excitonic amplitudes we obtain two equations (see, for example, [15])

$$\frac{dY_{slow,r}}{dt} - \left(\frac{Y_{slow,r}}{dt}\right)_{irrev} = F(t),$$

$$\frac{dY_{slow,nr}}{dt} - \left(\frac{Y_{slow,nr}}{dt}\right)_{irrev} = F(t), \quad (58)$$

where

$$\left(\frac{Y_{slow,r,nr}}{dt}\right)_{irrev} = -\frac{1}{\tau_{r,nr}} Y_{slow,r,nr}. \quad (59)$$

The above equations can be solved by means of Green's function, satisfying the equation

$$\frac{dG(t,u)}{dt} + \frac{1}{\tau} G(t,u) = -\delta(t-u), \quad (60)$$

with the solution

$$G(t,u) = \frac{\tau}{2} e^{-(1/\tau)|t-u|}. \quad (61)$$

Thus, the solutions of (57,58) have the form

$$Y_{slow}(t) = \int_{-\infty}^{\infty} F(u) G(t,u) dt'. \quad (62)$$

Using the pulse shape (57) we calculate the amplitudes Y_{slow}. In the lowest approximation we obtain

$$Y_{slow} \approx F_{max} \frac{\tau}{2} \exp\left(-\frac{|t|}{\tau}\right). \quad (63)$$

Using the expression (63) for radiative- and non-radiative decays, we calculate the susceptibility and the absorption coefficient , where the time dependent term has the form

$$\alpha \propto \frac{f_S M_{0,GS}^2}{\Gamma_{GS}} \exp\left(-\frac{1}{\tau_{S,r}}|t|\right) + B_S \exp\left(-\frac{1}{\tau_{S,nr}}|t|\right), \quad (64)$$

where B_{GS} is a certain constant. Quite analogous expression holds for the excited state. The same equations, with appropriate parameters, hold for the H and L excitons. The decline times $\tau_{r,nr}$ follow from the relation

$$\tau_{r,nr} = \frac{\hbar}{\Gamma_{r,nr}}. \quad (65)$$

The quantities Γ are given in Table 4. Below we give, as example, the formula for emission for the NPL with size 29 × 8 (interval).

$$\alpha = \frac{6}{(2475-\hbar\omega)^2+6}\left[\begin{array}{l}\exp(-3.67|t|)+\\ \exp(-0.003|t|)\end{array}\right]$$

$$+\frac{40}{(2486.7-\hbar\omega)^2+110}[\exp(-10.94|t|) \quad (66)$$

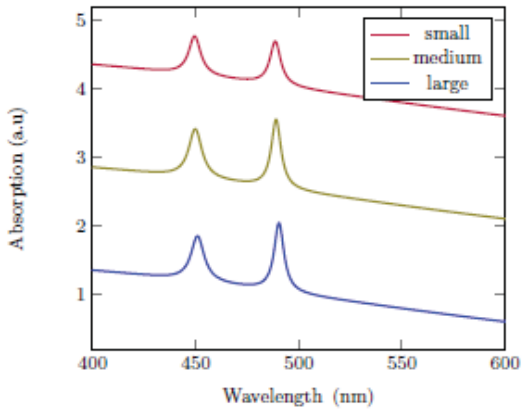

Figure 13 Normalized absorption for the case 'Lateral area' at 273 K.

TABLE 6. Sizes and exciton states energies, transition matrix elements M_{0SH}, oscillator strengths, and damping parameters, for disks analyzed by Brumberg *et al*. [12], lengths in nm, wave length in nm, matrix elements M_{0SH} in e × nm, energies in meV, the energy gap at room temperature 1750 meV, damping parameter Γ from Eq. (53) notation: 1: 56 × 41; 3ML, 2: 17 × 15; 4ML 3: 30 × 11; 5ML, 4: 17 × 15; 4ML, 5: 30 ×11; 4ML, 6: 56 × 41; 4ML.

Lat. extens.	1	2	3	4	5	6
$a^*_{e\|\|}$	1	1.26	1.553	1.26	1.26	1.26
r_{eff}	27	9	10.25	9	10.25	27
ρ_{eff}	27	7.15	6.6	7.15	8.134	21.455
$E_{res}(1SH)\lambda$	2843 437	2540 488.6	2381 521.2	2540 488.6	2537.7 489	2531 490.4
$E_{res}(1PH)\lambda$	2870 432	2558.48 484.6	2392.5 518.7			
$E_{res}(1SL)\lambda$	3201 388	2761 449.5	2533 490	2761 449.5	2758.7 449.8	2752 450.9
M_{0SH}	0.625	0.22	0.19	0.22	0.19	0.625
f_{SH}	4.16	4.77	5.47	4.77	4.6	4.96
f_{SL}	3.72	3.75	4.77	3.75	4.44	4.41
$\Gamma_{SH,r}$	4.63	2.53	2.86	2.53	2.86	2.86

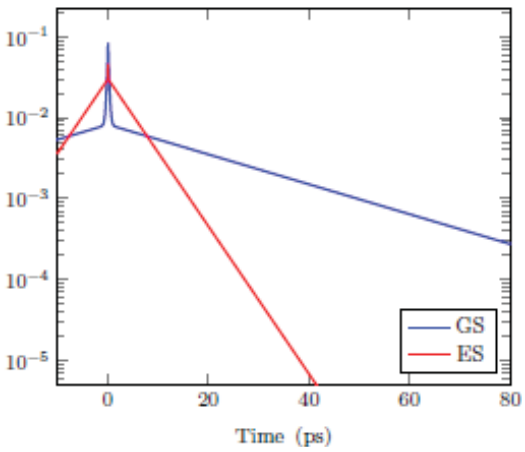

Figure 15 Evolution of the GS emission with time for 2 ps temporal bins, platelet size of 30 × 15 nm².

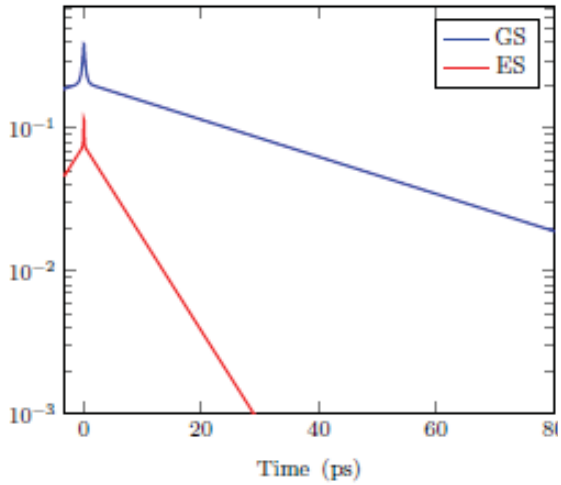

Figure 16 Evolution of GS emission with time for 2 ps temporal bins, platelet size 29 × 8 nm².

$$+\exp(-0.05|t|)].$$

It can be seen, that the log-time contributions are dominant. The excited state declines faster than the ground state. For times $t > 60$ *ps* only the ground state remains. The emission shape for 4 values of time is illustrated in **Figure 15**.

Making use of the expression (64), we have calculated the ES (red) and GS (blue) transients for different NPL sizes and the pulse shape (57). The results are presented in Figures 16-20. We have used the logarithmic scale. We notice the changes due to varying NPL sizes.

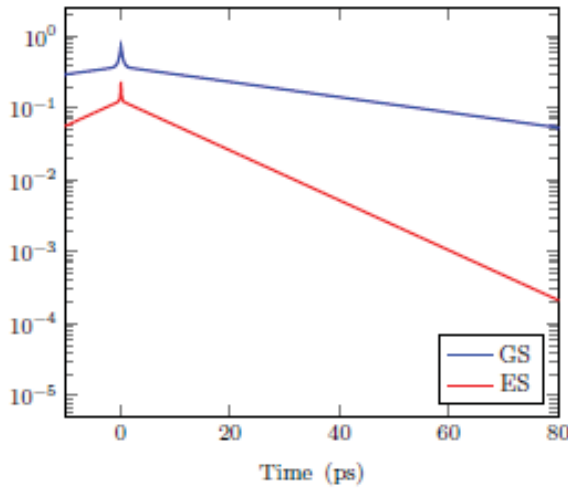

Figure 17 Evolution of the GS emission with time for 2 ps temporal bins, platelet size 21 × 7 nm².

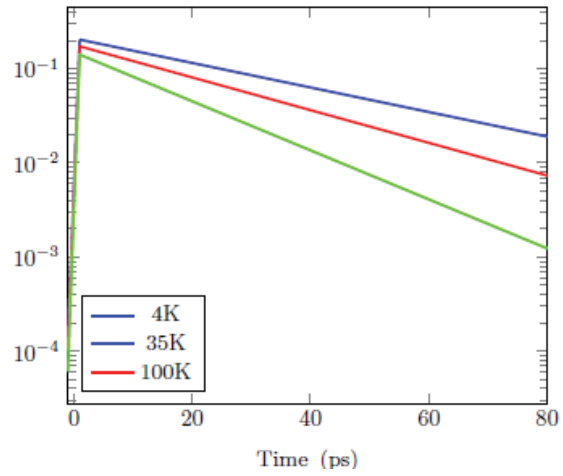

Figure 18 Evolution of the GS emission with time for 2 ps temporal bins at 4, 35, and 100 K, platelet size 29 × 8 nm².

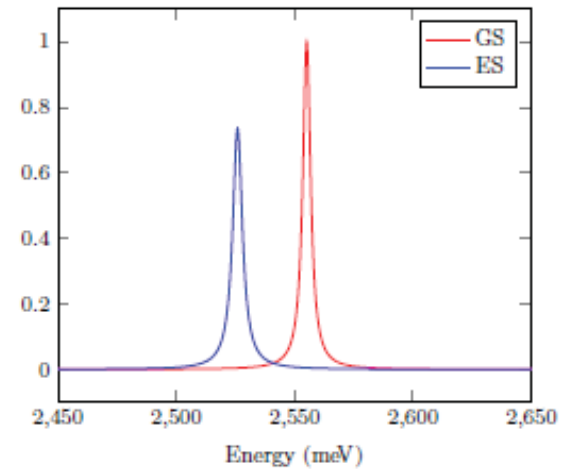

Figure 19 Evolution of the GS emission with time for 2 ps temporal bins at 4, 35, and 100 K, platelet size 41 × 13 nm².

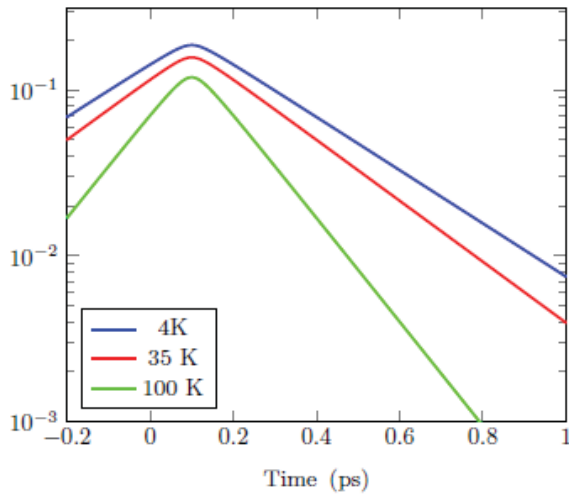

Figure 20 Evolution of GS emission with time for 2 ps temporal bins, platelet size of 29 × 8 nm².

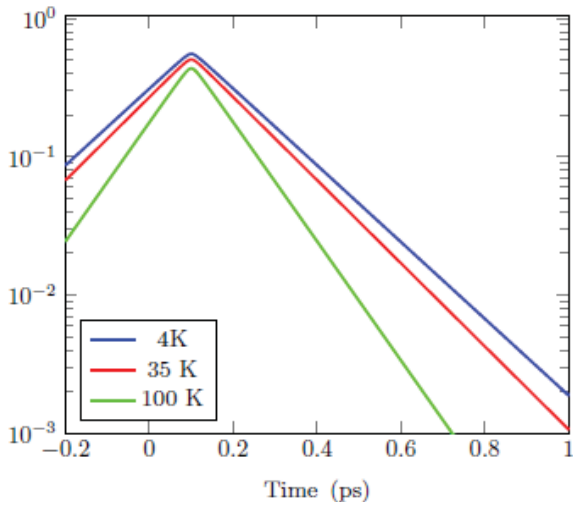

Figure 21 Evolution of GS emission with time for 2 ps temporal bins, platelet size 41 × 13 nm².

The discussion of the optical functions time dependence can be enlarged by including the temperature dependence. As is known, the general tendency is the increase of the damping parameters with temperature (see, for example,[23]). Since the radiative decline rate increases at least linearly with temperature, we assumed the formula

$$\Gamma_{GS,r} = \Gamma_{0,GS,r} + 10^{-2}\mathcal{T}, \tag{67}$$

with analogous expression for the excited state. The dependence of the non-radiative decay rates on temperature is, to our best knowledge,

not known. We assumed the following fit

$$\Gamma_{GS,nr} = \Gamma_{0,nr} + \frac{\mathcal{R} \times 10^{-4} \mathcal{T}^2}{\mathcal{T} + 235}, \quad (68)$$

where $\Gamma_{0,nr}$ is the value at 0 K. The same fit is assumed for the excited state. The effects of temperature are overlapping with the effects of varying NPL sizes. This is illustrated in **Figures** 19 and 20. The separation of radiative- and non-radiative declines is presented in **Figures** 21 and 22.

Conclusions

In this paper we have discussed some remarkable optical properties of CdSe monolayers systems. Atomically thin CdSe NPLs have unique physical properties which could be valuable for a broad range of applications [2], [24]. Strong light-matter interaction and atomically thin volume are advantages for 2D semiconductors which make them easy tunable, as the optical properties can be controlled using multiple modulation methods. The remarkable thinness of these materials also provides unique opportunities for engineering the excitonic properties. For example, changing the dielectric environment of NPLs significantly reduces the exciton binding energies and the free-particle band gap. With the help of RDMA, using dielectric potential resulting from the dielectric confinement, we have derived analytical expressions for the binding energy and absorption for NPLs depending on the monolayers number and lateral area. We also discussed the temperature and time dependence of the spectra, accounting for the radiative- and non-radiative decline rates. Our results have been thoroughly discussed and compared with the available experimental data showing a fairly good agreement. This approach and results may open up a variety of possibilities to manipulate excitonic states on the nanometer scale in 2D materials in the future.

Funding

The authors have no funding to declare.

Conflict of interest

The authors declare no conflicts of interest and have no competing interests.

Data availability statement

All data generated or analyzed during this study is included in this published article.

References

1. Ekimov A, Onushchenko A. Quantum size effect in 3-dimensional microscopic semiconductor crystals. JETP Lett. 1981;34:345.
2. Yu J, Chen R. Optical properties and applications of two-dimensional CdSe Nanoplatelets. InfoMat. 2020;2:905.
3. Dutta A, Medda A, Patra A. Recent advances and perspectives on colloidal semiconductor Nanoplatelets for optoelectronic applications. The Journal of Physical Chemistry C. 2021;125:20.
4. Murray CB, Norris DJ, Bawendi MG. Synthesis and characterization of nearly monodisperse CdE (E = S, Se, Te) semiconductor nanocrystallites. J Am Chem Soc. 1993;115:8706.
5. Joo J, Son JS, Kwon SG, Yu JH, Hyeon T. Low-temperature solution-phase synthesis of quantum well structured CdSe nanoribbons. J Am Chem Soc. 2006 May 3;128(17):5632-3. doi: 10.1021/ja0601686. PMID: 16637619.
6. Benchamekh R, Gippius NA, Even J. Tight-binding calculations of image-charge effects in colloidal nanoscale platelets of CdSe. Phys Rev B. 2014;89:035307.
7. Zelewski SJ, Nawrot KC, Zak A, Gladysiewicz M, Nyk M, Kudrawiec R. Exciton Binding Energy of Two-Dimensional Highly Luminescent Colloidal Nanostructures Determined from Combined Optical and Photoacoustic Spectroscopies. J Phys Chem Lett. 2019 Jun 20;10(12):3459-3464. doi: 10.1021/acs.jpclett.9b00591. Epub 2019 Jun 10. PMID: 31180226.
8. Shornikova EV, Yakovlev DR, Gippius NA, Qiang G, Dubertret B, Khan AH, Di Giacomo A, Moreels I, Bayer M. Exciton Binding Energy in CdSe Nanoplatelets Measured by One- and Two-Photon Absorption. Nano Lett. 2021 Dec 22;21(24):10525-10531. doi: 10.1021/acs.

nanolett.1c04159. Epub 2021 Dec 7. PMID: 34874734; PMCID: PMC8886564.

9. Achtstein AW, Schliwa A, Prudnikau A, Hardzei M, Artemyev MV, Thomsen C, Woggon U. Electronic structure and exciton-phonon interaction in two-dimensional colloidal CdSe nanosheets. Nano Lett. 2012 Jun 13;12(6):3151-7. doi: 10.1021/nl301071n. Epub 2012 May 29. PMID: 22625408.

10. Chakrabarti P, Morin K, Lagarde D, Marie X, Boulier T. Direct Measurement of the Lifetime and Coherence Time of Cu_{2}O Rydberg Excitons. Phys Rev Lett. 2025 Mar 28;134(12):126902. doi: 10.1103/PhysRevLett.134.126902. PMID: 40215532.

11. Baghdasaryan DA, Harutyunyan VA, Hayrapetyan DB, Kazaryan EM, Baskoutas S, Sarkisyan HA. Exciton States and Optical Absorption in CdSe and PbS Nanoplatelets. Nanomaterials (Basel). 2022 Oct 20;12(20):3690. doi: 10.3390/nano12203690. PMID: 36296880; PMCID: PMC9611409.

12. Brumberg A, Harvey SM, Philbin JP, Diroll BT, Lee B, Crooker SA, Wasielewski MR, Rabani E, Schaller RD. Determination of the In-Plane Exciton Radius in 2D CdSe Nanoplatelets via Magneto-optical Spectroscopy. ACS Nano. 2019 Aug 27;13(8):8589-8596. doi: 10.1021/acsnano.9b02008. Epub 2019 Jun 28. PMID: 31251582.

13. Ziemkiewicz D, Knez D, Garcia EP, Zielińska-Raczyńska S, Czajkowski G, Salandrino A, Kharintsev SS, Noskov AI, Potma EO, Fishman DA. Two-photon absorption in silicon using the real density matrix approach. J Chem Phys. 2024 Oct 14;161(14):144117. doi: 10.1063/5.0219329. PMID: 39392143.

14. Ziemkiewicz D, Czajkowski G, Zieli´nska-Raczy´nska S. Optical properties of Rydberg excitons in Cu2O-based superlattices. Phys. Rev. B 2024; 109: 085309.

15. Karpinski K, Czajkowski G. Dynamics of Cu2O Rydberg excitons – real density matrix approach. Open Accsess J Phys Math. 2025;1(2):01.

16. Ziemkiewicz D, Czajkowski G, Zieli´nska-Raczy´nska S. Optical properties of excitons in CdSe nanoplatelets and disks: real density matrix approach. arXiv 2024;2406.01144v1 [physics.optics]: 3 Jun. 4.

17. Chuu DS, Hsiao CM, Mei WN. Hydrogenic impurity states in quantum dots and quantum wires. Phys Rev B Condens Matter. 1992 Aug 15;46(7):3898-3905. doi: 10.1103/physrevb.46.3898. PMID: 10004117.

18. Ziemkiewicz D, Czajkowski G, Karpi´nski K, Zieli´nska-Raczy´nska S. Excitonsin Cu_2O: From quantum dots to bulk crystals and additional boundary conditions for Rydberg exciton-polaritons. Phys. Rev. B 2020; 101: 205202.

19. Abramowitz M, Stegun I. Handbook of Mathematical Functions. Dover Publications, New York. 1965.

20. Landau LD, Lifshitz EM. Electrodynamics of continuous Media. In: Lifshitz EM, Pitaevskii LP editors. 2nd ed. Pergamon Press, Oxford; 1984.

21. Caicedo DS, Caprioglio P, Lehmann F. Effects of quantum and dielectric confinement on the emission of Cs-Pb-Br composites. Adv Func Mater. 2023;33:2305240.

22. Quanqin D, Yanli S, Dongmei L, et al. Temperature dependence of band gap in CdSe nanocrystals. Chemical Physics Letters. 2007;439:65. doi: 10.1016/j.cplett.2007.03.034.

23. Zhao H, Wachter S, Kalt H. Effect of quantum confinement on exciton-phonon interactions. Phys Rev B. 2002;42:11218.

24. Bai P, Hu A, Deng Y, Tang Z, Yu W, Hao Y, Yang S, Zhu Y, Xiao L, Jin Y, Gao Y. CdSe/CdSeS Nanoplatelet Light-Emitting Diodes with Ultrapure Green Color and High External Quantum Efficiency. J Phys Chem Lett. 2022 Oct 6;13(39):9051-9057. doi: 10.1021/acs.jpclett.2c02633. Epub 2022 Sep 25. PMID: 36153736.